

## Electronic Structures of Tungsten and Molybdenum Carbides as a Fuel Cell Anode Catalyst

Hiroyuki Tominaga\* and Masatoshi Nagai

Graduate School of Bio-applications and Systems  
Engineering, Tokyo University of Agriculture and  
Technology, 2-24 Nakamachi, Koganei, Tokyo 184-8588

Received July 2, 2010  
E-mail: tomi@cc.tuat.ac.jp

The band structures of  $W_2C(001)$ ,  $WC(001)$ ,  $\beta$ - $Mo_2C(001)$ , and  $Pt(111)$  slabs as an anode catalyst with two adsorbed hydrogen molecules using periodic DFT calculations revealed the anode performance of the carbides.

Polymer electrolyte fuel cells (PEFCs) are a promising technology for solving the problems of energy shortages and global warming in the future; devices which run on these types of cells use a cleaner energy-conversion than those running on fossil fuels. Platinum-containing catalysts are available as electrode catalysts for the PEFCs, but they are quite expensive. Alternatives to Pt catalysts are being developed by many researchers based on experimental or theoretical studies. Although many of these studies are concerned with the cathode catalyst, little attention has been given to studies concerning anode catalysts. Transition-metal carbides are chemically inert in acidic solutions and their catalytic behavior is similar to platinum catalysts, therefore they are suitable for electrode applications. Tungsten<sup>1,2</sup> and molybdenum<sup>2</sup> carbides have been used as alternative electrode catalysts. We have experimentally investigated tungsten and molybdenum and their bimetallic carbides as an anode catalyst in previous studies.<sup>3,4</sup> A recent significant improvement in the performance of low-cost computers has allowed extensive studies of catalysts and catalysis, the catalytic properties of hydrogen adsorption on tungsten carbide,<sup>5</sup> and hydrogen oxidation on Pt.<sup>6</sup> In a previous paper,<sup>7</sup> the density of states (DOS) of the adsorbed oxygen and the Fermi level of the cathode catalyst were studied for tungsten nitrides as a cathode catalyst that involved the band structure. The DOS and Fermi level are essential for cathode performance. Nørskov and his co-workers<sup>8–10</sup> studied surface properties using the d-band center which is calculated as the first moment of the d-band DOS on the surface atoms referenced to the Fermi level. The correlation between oxygen reduction reaction (ORR) activity and the d-band center was calculated as the average of the Pt atoms in the two top layers of the projected DOS of the oxygen atoms on  $Pt(111)$ . Lima et al.<sup>11</sup> reported a correlation between the d-band center and the kinetics of the ORR and revealed a volcano-type dependence. Thus, the band structure could possibly reveal electrode

catalytic properties. However, there are few studies of anode catalysts using the band structure. In this study, we calculated the band structure in order to estimate the properties of the tungsten and molybdenum carbide slabs as an anode catalyst. We also discuss the band structure of the  $Pt(111)$  slab for comparison.

Self-consistent, gradient-corrected, periodic DFT calculations were performed using the Vienna Ab-initio Simulation Package (VASP).<sup>12–15</sup> The calculations were performed using the projector-augmented wave (PAW) method<sup>16,17</sup> and generalized gradient approximation (GGA) corrections as proposed by Perdew et al.<sup>18</sup> For the plane wave set, a cutoff energy of 680 eV was used. The convergence criteria for the energy calculation and structure optimization were set to an SCF tolerance of  $1.0 \times 10^{-6}$  eV and a maximum force tolerance of  $0.02 \text{ eV } \text{\AA}^{-1}$ . The conformations of the models used for the calculation of the catalysts ( $W_2C(001)$ ,  $WC(001)$ ,  $\beta$ - $Mo_2C(001)$ , and  $Pt(111)$ ) are the  $W_{32}C_{16}$ -5-layers,  $W_{24}C_{24}$ -4-layers,  $Mo_{24}C_{12}$ -3-layers, and  $Pt_{36}$ -3-layers, respectively. For the calculation of the band structure, the geometry was initially optimized by restricting the Brillouin zone of the  $\Gamma$  point, and then the calculation was done using 15 k-point samplings through  $\Gamma(0,0,0) \rightarrow X(0.5,0,0) \rightarrow M(0.5,0.5,0) \rightarrow \Gamma(0,0,0)$ . The reliability for the VASP calculation was reported in a previous paper.<sup>7</sup>

A geometry optimization was performed to investigate the adsorption behavior of hydrogen as a reactant on the anode electrode. Two hydrogen molecules were placed at  $1.0 \text{ \AA}$  for optimization on the top position of the surface W atoms on the  $W_2C(001)$  slab and 3-fold positions of the surface atoms on the  $WC(001)$ ,  $\beta$ - $Mo_2C(001)$ , and  $Pt(111)$  slabs. The optimized structures of hydrogen on each slab with the DOSs of each hydrogen atom ( $H_s$  DOS) are shown in Figure 1. All of the hydrogen molecules on the  $W_2C(001)$ ,  $WC(001)$ ,  $\beta$ - $Mo_2C(001)$ , and  $Pt(111)$  slabs were dissociated after optimization. For the  $W_2C(001)$  slab, the hydrogen atoms were mostly adsorbed on the bridge position of the surface W atoms. All the hydrogen atoms on the  $WC(001)$  slab were adsorbed on the 3-fold positions of the surface W atoms without ( $H1$  and  $H2$ ) and with ( $H3$  and  $H4$ ), the underlying C atom of the second layer. The hydrogen atoms on the  $\beta$ - $Mo_2C(001)$  slab were also adsorbed on the 3-fold positions of the surface Mo atoms without ( $H1$ ,  $H2$ , and  $H4$ ) and with ( $H3$ ), the underlying C atom of the second layer. For the  $Pt(111)$  slab, the  $H1$  and  $H2$  were adsorbed on the bridge positions of the surface Pt atoms, and the  $H3$  and  $H4$  were adsorbed on the top position of the surface Pt atoms. Gaston et al.<sup>5</sup> investigated the adsorption structures of hydrogen on the tungsten carbide. They reported that the hydrogens were adsorbed on the 3-fold sites of the surface atoms, and the height of the hydrogens from the surface tungsten atoms was in the range of  $1.057$ – $1.126 \text{ \AA}$ . These results agreed with our calculated results, i.e., the hydrogens were adsorbed on the 3-fold site of the  $WC(001)$  slab with the height in the range of  $1.054$ – $1.124 \text{ \AA}$ .

Regarding the  $H_s$  DOS, the  $H_s$  DOSs for the  $W_2C(001)$  and  $Pt(111)$  slabs were distributed with broad peaks, while those for the  $WC(001)$  and  $\beta$ - $Mo_2C(001)$  slabs were distributed with sharp peaks. These results implied that the electron of the hydrogen on the  $W_2C(001)$  and  $Pt(111)$  slabs was delocalized, while that on the  $WC(001)$  and  $\beta$ - $Mo_2C(001)$  slabs was

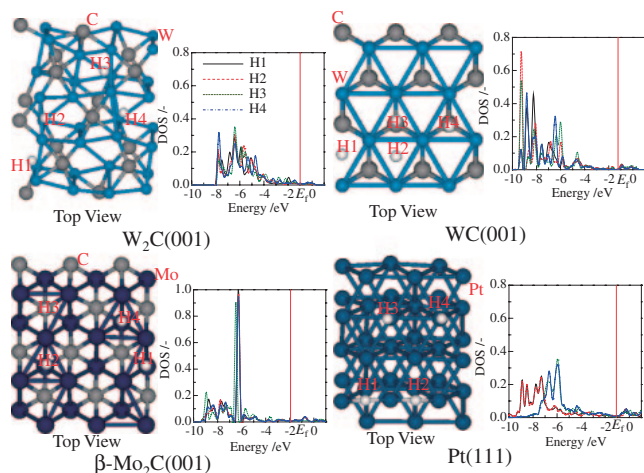


**Figure 1.** Optimized structures of the two hydrogen molecules on the  $W_2C(001)$ ,  $WC(001)$ ,  $\beta\text{-Mo}_2C(001)$ , and  $Pt(111)$  slabs with the density of states of the H-s orbitals.  $E_f$  is the Fermi level.

localized. Thus, the electron of the hydrogen adsorbed on the 3-fold positions of the surface atoms tends to be localized. The maximum intensities of the H-s DOS peak on the  $W_2C(001)$ ,  $WC(001)$ ,  $\beta\text{-Mo}_2C(001)$ , and  $Pt(111)$  slabs were 0.351, 0.712, 1.104, and 0.354, respectively, and their Hs' 1s orbital coefficients were 0.038, 0.064, 0.077, and 0.049, respectively. As a result, the higher intensity of the H-s DOS has the higher 1s orbital coefficient of hydrogen. This indicates that the energetic localization corresponded to the spatial localization of the electron. The electron of hydrogen on the  $W_2C(001)$  and  $Pt(111)$  slabs can more easily move than that on the  $WC(001)$  and  $\beta\text{-Mo}_2C(001)$  slabs, because the localized electron is strictly bound in an atomic nucleus. Since the hydrogen releases the electron to become a hydron ( $H \rightarrow H^+ + e^-$ ) on the anode electrode, the delocalized electron is more desirable for an anode catalyst. Therefore, the  $W_2C(001)$  and  $Pt(111)$  slabs are more suitable as an anode catalyst than the  $WC(001)$  and  $\beta\text{-Mo}_2C(001)$  slabs. This suggestion corresponds to the experimental results of the  $I$ - $V$  power measurement,<sup>3,4</sup> i.e., the current densities of the  $Pt(111)$  and  $W_2C$  were higher than those of  $WC$  and  $\beta\text{-Mo}_2C$  as shown in Table 1. Consequently, the  $W_2C$  is superior to other carbide catalysts as an anode catalyst because of its adsorption structure of the hydrogens and the derived H-s DOS distribution. However, the distorted structure of the  $W_2C(001)$  slab after the adsorption of hydrogen molecules was supported by the XRD data in that the  $W_2C$  crystal was amorphous. This shows that the  $W_2C$  was not durable, but the  $W_2C$  was formed together with the  $WC$  crystal under the same experimental conditions, which was more durable than the  $W_2C$  alone while maintaining high anode performance.

In the four-electron reaction ( $2H_2 + O_2 \rightarrow 2H_2O$ ), a hydrogen releases an electron to become a hydron ( $H \rightarrow H^+ + e^-$ ) in the anode electrode, then the electron transfers to the cathode electrode. According to the band structure theory, current flow is caused by a conduction electron moving freely along the conduction band near the Fermi level. Thus, an electron placed near the Fermi level of the anode catalyst transfers to the

**Table 1.** Obtained Current Densities by  $I$ - $V$  Power Measurements and Fermi Levels of the Clean ( $E_f$  Clean),  $2H_2$  Adsorbed ( $E_{f-A}$ ) and  $O_2$  Adsorbed ( $E_{f-C}$ ) Slabs with the Values of  $E_{f-A} + E_0$

	Current density <sup>a)</sup> /mA cm <sup>-2</sup>	$E_f$ clean /eV	$E_{f-A}$ /eV	$E_{f-C}$ /eV	$E_{f-A} + E_0$ <sup>b)</sup> /eV
$W_2C(001)$	5.0	-0.892	-0.996	—	-0.946
$WC(001)$	0.7	-1.507	-1.225	—	-1.035
$\beta\text{-Mo}_2C(001)$	0.15	-2.036	-1.932	—	-1.146
$Pt(111)$	60.5	-1.220	-1.080	-1.167	-1.010

a) Current density at 0.7 V in the  $I$ - $V$  curve.<sup>3,4</sup> b)  $E_0$  = (electric charge of an electron)  $\times$  (peak position of the cyclic voltammograms).

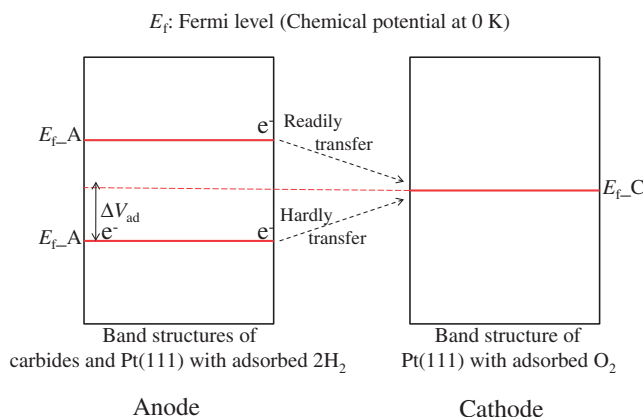


**Figure 2.** An illustration of electron transfer from the anode electrode to the cathode electrode.  $E_{f-A}$  is the Fermi level of the anode catalyst slab with adsorbed  $2H_2$ .  $E_{f-C}$  is the Fermi level of the cathode catalyst slab with adsorbed  $O_2$ .

conduction band near the Fermi level of the cathode catalyst during the four-electron reaction. The Fermi level is the same as the chemical potential at 0 K. Therefore, the electrochemical potential of an electron placed near the Fermi level has almost the same value as the Fermi level. An electron readily transfers from the higher position of the electrochemical potential to the lower position as illustrated in Figure 2. Thus, the higher Fermi level of the anode catalyst slab with the adsorbed  $2H_2$  ( $E_{f-A}$ ) than that of the cathode catalyst slab with the adsorbed  $O_2$  ( $E_{f-C}$ ) is suitable as an anode catalyst, because an electron readily transfers from the anode electrode to the cathode electrode. For the case when the  $E_{f-A}$  is lower than the  $E_{f-C}$ , an electron hardly transfers from the anode electrode to the cathode electrode. However, since the energy of an electron depends on the electrochemical potential (Energy = (electric charge)  $\times$  (electric potential)), the electron is able to transfer from the anode electrode to the cathode electrode when the electrochemical potential of the electron exceeds the  $E_{f-C}$  by obtaining an additional electric potential ( $\Delta V_{ad}$ ) (Figure 2). The  $E_{f-A}$  and Fermi level values of the clean  $W_2C(001)$ ,  $WC(001)$ ,  $\beta\text{-Mo}_2C(001)$ , and  $Pt(111)$  slabs are listed in Table 1. For  $Pt(111)/C$  as the cathode electrode, the  $E_{f-C}$  value (-1.167 eV) of  $Pt(111)$  is also shown in Table 1. The Fermi level of the  $W_2C(001)$  slabs became lower after the  $2H_2$

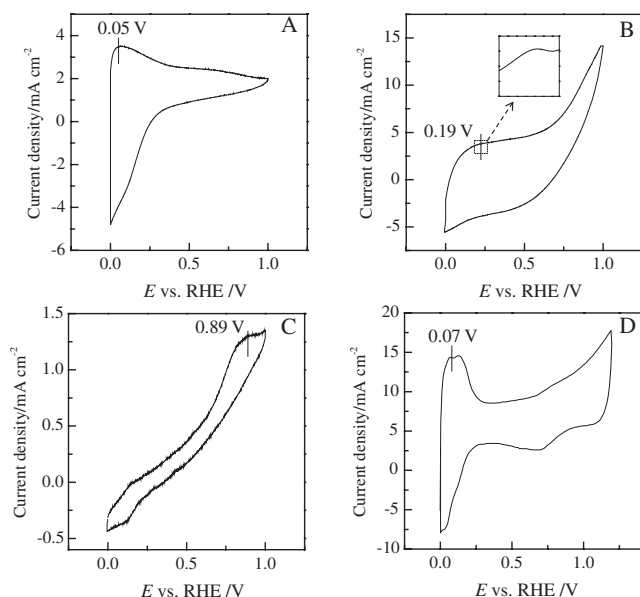


**Figure 3.** The cyclic voltammograms of the (A) W<sub>2</sub>C, (B) WC, (C)  $\beta$ -Mo<sub>2</sub>C, and (D) Pt(111).

adsorption, while that of the other slabs became higher after the 2H<sub>2</sub> adsorption. The  $E_{f-A}$  values of the W<sub>2</sub>C(001) and Pt(111) slabs were  $-0.996$  and  $-1.080$  eV, respectively. These values already exceeded the  $E_{f-C}$  value of the Pt(111) slab, and the obtained current densities were high in comparison to the WC(001) and  $\beta$ -Mo<sub>2</sub>C(001) slabs whose  $E_{f-A}$  values were below the  $E_{f-C}$  value of the Pt(111) slab. In particular, the  $E_{f-A}$  of the  $\beta$ -Mo<sub>2</sub>C(001) slab had the greatest difference from the  $E_{f-C}$  of the Pt(111) slab, and thus, the current density was the lowest among all the slabs. These results showed that the  $E_{f-A}$  value higher than  $E_{f-C}$  was suitable as an anode catalyst, and corresponded to the suggestion mentioned above. Therefore, the W<sub>2</sub>C(001) was the most suitable anode catalyst among the three carbides with respect to the  $E_{f-A}$  value.

Figure 3 shows a cyclic voltammogram of the W<sub>2</sub>C, WC,  $\beta$ -Mo<sub>2</sub>C, and Pt(111). The details of the experimental methods have been reported in previous studies.<sup>3,4</sup> The peak position of the cyclic voltammogram denotes the redox potential in a redox reaction ( $\text{Red} \rightleftharpoons \text{Ox} + ne^-$ ). At this position, many electrons transfer to the cathode electrode during the anode sweep. Thus, the  $\Delta V_{ad}$  value, as discussed above and shown in Figure 2, was estimated by this peak position. For the W<sub>2</sub>C and Pt(111), the peaks of the cyclic voltammogram were observed at 0.05 and 0.07 V, respectively. This shows that the electron transfers toward the cathode electrode as soon as the anode sweep starts. The  $E_{f-A}$  values of the W<sub>2</sub>C(001) and Pt(111) slabs are greater than the  $E_{f-C}$  of the Pt(111) slab as mentioned above, and thus, no or a slight additional  $\Delta V_{ad}$  is required. These calculated results were supported by the experimental results of the low peak positions in the cyclic voltammogram. On the other hand, the  $E_{f-A}$  of the WC(001) and  $\beta$ -Mo<sub>2</sub>C(001) slabs are lower than the  $E_{f-C}$  of the Pt(111) slab, and an additional  $\Delta V_{ad}$  is

required in order to transfer an electron from the anode electrode to the cathode electrode. The cyclic voltammogram peaks of the WC(001) and  $\beta$ -Mo<sub>2</sub>C(001) slabs were observed at 0.19 and 0.89 V, respectively. When an electron placed near the  $E_{f-A}$  of the WC(001) and  $\beta$ -Mo<sub>2</sub>C(001) slabs gains these voltages, the energies of the electron are greater than the  $E_{f-C}$  of the Pt(111) slab on both slabs as listed in Table 1 (the values of  $E_{f-A} + E_0$ ), and the electron begins to transfer toward the cathode electrode. These results supported the suggestion proposed above. In an actual fuel cell, this  $\Delta V_{ad}$  would be part of the internal resistance and lead to low current density. The measured  $I$ - $V$  power supports this suggestion because the obtained current density of the  $\beta$ -Mo<sub>2</sub>C was the lowest and the  $\Delta V_{ad}$  value was the highest of all as shown in Table 1.

In conclusion, theoretical studies revealed that the anode performance of W<sub>2</sub>C(001), WC(001),  $\beta$ -Mo<sub>2</sub>C(001), and Pt(111) slabs are based on the following two factors: (1) the adsorption structure of the hydrogen on the slab and the derived electronic structure of the hydrogen, and (2) the  $E_{f-A}$  value of the carbides and Pt(111). The W<sub>2</sub>C(001) slab was the most suitable among the three carbides as an anode catalyst with respect to these two factors. The calculation in this study corresponded to the experimental results of which W<sub>2</sub>C shows high anode performance.

## References

- 1 D. V. Sokolsky, V. Sh. Palanker, E. N. Baybatyrov, *Electrochim. Acta* **1975**, *20*, 71.
- 2 T. Morishita, Y. Soneda, H. Hatroi, M. Inagaki, *Electrochim. Acta* **2007**, *52*, 2478.
- 3 M. Nagai, M. Yoshida, H. Tominaga, *Electrochim. Acta* **2007**, *52*, 5430.
- 4 S. Izhar, M. Nagai, *J. Power Sources* **2008**, *182*, 52.
- 5 N. Gaston, S. Hendy, *Catal. Today* **2009**, *146*, 223.
- 6 T. Zhang, A. B. Anderson, *J. Phys. Chem. C* **2007**, *111*, 8644.
- 7 H. Tominaga, M. Nagai, *Electrochim. Acta* **2009**, *54*, 6732.
- 8 B. Hammer, J. K. Nørskov, *Adv. Catal.* **2000**, *45*, 71.
- 9 J. R. Kitchin, J. K. Nørskov, M. A. Barteau, J. G. Chen, *J. Chem. Phys.* **2004**, *120*, 10240.
- 10 V. Stamenkovic, B. S. Mun, K. J. J. Mayrhofer, P. N. Ross, N. M. Markovic, J. Rossmeisl, J. Greeley, J. K. Nørskov, *Angew. Chem., Int. Ed.* **2006**, *45*, 2897.
- 11 F. H. B. Lima, J. Zhang, M. H. Shao, K. Sasaki, M. B. Vukmirovic, E. A. Ticianelli, R. R. Adzic, *J. Phys. Chem. C* **2007**, *111*, 404.
- 12 G. Kresse, J. Hafner, *Phys. Rev. B* **1993**, *47*, 558; G. Kresse, J. Hafner, *Phys. Rev. B* **1994**, *49*, 14251.
- 13 G. Kresse, Thesis, Technische Universität Wien, **1993**.
- 14 G. Kresse, J. Furthmüller, *Comput. Mater. Sci.* **1996**, *6*, 15.
- 15 G. Kresse, J. Furthmüller, *Phys. Rev. B* **1996**, *54*, 11169.
- 16 P. E. Blöchl, *Phys. Rev. B* **1994**, *50*, 17953.
- 17 G. Kresse, D. Joubert, *Phys. Rev. B* **1999**, *59*, 1758.
- 18 J. P. Perdew, J. A. Chevary, S. H. Vosko, K. A. Jackson, M. R. Pederson, D. J. Singh, C. Fiolhais, *Phys. Rev. B* **1992**, *46*, 6671.